Mechanics & Industry **18**, 220 (2017)

DOI: 10.1051/meca/2016042
www.mechanics-industry.org

Mechanics & Industry

Optimization of CO_2 laser welding process parameters of PP/EPDM/Clay nanocomposite using response surface methodology

A. Ahmadi[1], N.B. Mostafa Arab[a1], Gh. Naderi[2] and M.R. Nakhaei[1]

[1] Faculty of Mechanical Eng., Shahid Rajaee Teacher Training University, Tehran, Iran
[2] Iran Polymer and Petrochemical Institute, Tehran, Iran

Received 8 May 2015, Accepted 27 August 2016

Abstract – In recent years, polymer – based nanocomposites have found wide applications in various industries. Polypropylene / ethylene – propylene - diene monomer /Nanoclay (PP/EPDM/Nanoclay) nanocomposite is one of these materials that has many applications in automotive and aircraft industries. Welding as a fabrication process has attracted the attention of researchers for joining these materials. Among welding processes, laser welding because of its advantages can be a choice for joining of PP/EPDM/Nanoclay nanocomposites. In this paper, the effect of CO_2 laser power, scan velocity, stand-off distance and clay content on impact strength of butt-welded PP/EPDM/Nanoclay 3.2 mm sheets is investigated. The response surface methodology (RSM) is used to develop a statistical model relating the above parameters to the impact strength of the weld joint. The results indicated that increase in clay content and scan velocity decreased the impact strength whereas stand-off distance increased it. The maximum impact strength of 70 J/m is achieved at laser power of about 103 W, velocity of 400 mm.min^{-1}, stand-off-distance 8 mm and clay content of about 1.3% wt.

Key words: Polypropylene / ethylene-propylene-diene monomer / Nanoclay (PP/EPDM/Clay) / laser welding / impact strength / response surface methodology

1 Introduction

Polypropylene (PP) is a commodity thermoplastic polymer with a number of useful properties, including low density, high thermal stability, chemical resistance, high softening point, low cost, good processability and high strength. However, its ability to be utilized as an engineering thermoplastic is still limited by low modulus and poor impact resistance, especially at low temperatures. To increase impact strength of PP, some impact modification or rubbery materials such as ethylene-propylene rubber (EPR), ethylene-octane copolymer (EOC), and ethylene-propylene-diene monomer (EPDM) are added to PP matrix. The combination of PPs and rubbery material are called thermoplastic polyolefin (TPO). Among these rubbery materials, EPDM is a conventional impact modifier and is used widely because it improves impact resistance in a wide range of temperature in comparison to other impact modifiers. Due to the addition of elastomer, stiffness and mechanical strength of TPO are lower than pure PP. Since both stiffness and toughness are important for some applications; this issue is addressed via incorporation of nanoclay fillers to TPO matrix [1–3]. Therefore, TPO nanocomposites are a new class of materials that not only have improved mechanical properties than previous TPO, but have enhanced their applications for automotive parts and other industries [1, 3–5]. To date, these nanocomposites have been prepared successfully in different loading of PP, EPDM and nanoclay by many researchers to study their morphology, mechanical, physical and thermal properties [1–4, 6–8]. Investigations on their weldability and their successful welding are necessary to increase their application.

In recent years, conventional methods such as adhesives, fasteners, hot plate welding, ultrasonic or vibration welding have been established for joining thermoplastics and nanocomposites [9–11]. Laser welding is also a thermal bonding technique that has received considerable attention as a promising joining technology with high quality, high speed and good precision [12, 13]. This process can also be used easily for good flexibility, non contact, full automation and etc.

[a] Corresponding author: n.arab@srttu.edu

Bates et al. used vibration welding to bond PP/clay nanocomposites with different amounts of clay content. They found that strength of the bond decreased with increasing clay content [10].

Mokhtarzadeh et al. investigated hot plate welding of PP/clay nanocomposites utilizing 0, 3 and 6% wt clay. They found that the significant parameters for obtaining good welds were heating phase (temperature and time) and welding pressure. They also concluded that the clay content had a negative effect on weld strength [11].

Dosser et al. welded carbon nanocomposites with Direct-Diode and Nd:YAG solid state lasers. Their findings demonstrated that the same methods can be used for welding of carbon nanocomposite and carbon black filled materials [12].

Nakhaei et al. [13] conducted experiments on laser welding of PP/clay nanocomposites to determine optimal welding parameters. Their results show that tensile strength of the weld joint deacreased with increase in clay content and welding speed.

Survey of the past literature shows that there are no reports available as such for laser welding of TPO nanocomposites. Therefore, the aim of this work is on studying the weldability of TPO nanocomposites. For this purpose, the response surface methodology (RSM) is utilized to predict the effect of clay content and key CO_2 laser welding parameters (laser power, welding velocity and stand-off-distance) on impact strength of butt welds in 3.2 mm thick sheets of TPO nanocomposites. The developed statistical model relates the input to output variables and optimizes the response to achieve the desired weld quality. Adequacy of the model is verified by comparison of the experimental and predicted results.

2 Response surface methodology

Response surface methodology is a collection of mathematical and statistical techniques for analyzing the relationship between one and more response variables and a set of input variables or factors. This technique uses a number of input variables and their levels to represent several experiments in which each experiment consists of a set of factors. Then RSM develops an appropriate approximating mathematical model with best fits to response. This model can be expressed by:

$$y = f(x_1, x_2, \ldots, x_k) \tag{1}$$

where y is response and $x_1, x_2, \ldots, x_k$ are measurable input variables.

This model can predict response of each set of factors in the range of selected variables that are not present in the design matrix. So, it can also determine values of input variables that produce desirable values (optimized values) of the response.

The selected model can be linear, linear and squared, linear and interactions, or a full quadratic model. Usually, a second-order polynomial Equation (2) is used in RSM [14].

$$y = \beta_0 + \sum_{i=1}^{k} \beta_i x_i + \sum_{i=1}^{k} \beta_{ii} x_i^2 + \sum_{i=1}^{k-1} \sum_{j=2}^{k} \beta_{ij} x_i x_j \tag{2}$$

where β_i, β_{ii}, β_{ij} are called the regression coefficient and β_0 is a constant parameter.

Table 1. Impact strength of TPO blend and nanocomposites.

Sample code	TPO	TPO3	TPO6
Impact strength (J/m)	85 ± 0.7	81.2 ± 0.6	71.3 ± 0.8

3 Materials and experimental procedure

3.1 Raw material

The base materials for the nanocomposites were: (a) polypropylene(PP) grade Z30S from Arak Petrochemical co. of Iran with density = 0.91 g.cm^{-3} and MFR at 230 °C, 2.16 Kg = 25 g/10 min, (b) Ethylene-propylene-Diene-Monomer(EPDM) with a commercial grade(KEP 270) from Korea Kumho polychem with density 0.086 g.cm^{-3} and Mooney viscosity ML(1+4)125 °C = 60 M, 68% ethylene and 4.5% ENB content, (c) carbon black 330 from Bayer co. of Germany. (d) the nanoclay used in the nanocomposite was Cloisite 15A from Sothern clay products, a natural montmorillonite modified with a dimethyl hydrogenated tallow quaternary ammonium having a cation exchange capacity of 125 meqniv/100 g and density of 1.66 g.cm^{-3}.

3.2 Nanocomposite preparation

In order to prepare TPO nanocomposites, combination of PP, EPDM, nanoclay and 0.5% wt carbon black (for better absorption of laser light) were mixed in a haake internal mixer (Germany) for 10 minutes at a temperature of 180 °C and rotor speed of 60 rpm. Three different PP/EPDM/nanoclay nanocomposites containing 0, 3, 6 wt% nanoclay were prepared (TPO, TPO3, TPO6). The composition of PP and EPDM in all TPO nanocomposites was fixed at 80/20 PP/EPDM (wt/wt). The resulting materials were hot pressed at 200 °C for 10 min. using a Mini Test Press operating at 22 MPa to obtain sheets with an average thickness of 3.2 mm. TPO nanocomposite sheets of 200 mm × 160 mm × 3.2 mm dimension were used as work piece. The impact strength of the TPO nanocomposites are shown in Table 1. The impact test was performed according to standard D256 and reported values of impact strength are presented in Table 1 which are the average of at least three specimen measurements.

Fig. 1. Set up of laser welding equipment.

3.3 Equipment

A CO_2 laser with a maximum optical power of 120 W and 10640 nm wavelength was used. The diameter of the spot at the workpiece surface for stand-off-distances of 5, 6.5 and 8 mm were 0.9, 1.2, 1.5 mm, respectively. A fixture was applied to ensure the intimate contact between sheets and clamp them under pressure during the welding operation. The laser and CO_2 fixture are shown in Figure 1.

3.4 Selecting important process parameters and response

Based on the literature, the independent process parameters affecting the impact strength of TPO nanocomposite are identified as laser power, scan velocity, stand-off-distance and clay content in TPO nanocomposites [13–18].

3.5 Selecting limits of process parameters

A large number of trial runs were carried out to find out the feasible working limits of laser welding process parameters. Different combinations of process parameters were used to carry out the trial runs. This was carried out by varying one of the factors while keeping the rest of them at constant values. The working range of each process parameter was decided upon by inspecting the appearance of the weld seam for any visible defects such as overheating, decomposition of weld (Fig. 2) and depth of penetration. Range of the clay content in TPO nanocomposite was selected based on the past literature [10,11,13].

The level of the selected process parameters with their limit and notations are presented in Table 2.

Table 2. Process control parameters and their limits.

Parameters	Units	Notations	Limits		
			−1	0	+1
Clay	wt%	C	0	3	6
Laser power	Watt	P	80	100	120
Scan velocity	mm/min	V	400	750	1100
Stand-off-distance	mm	S	5	6.5	8

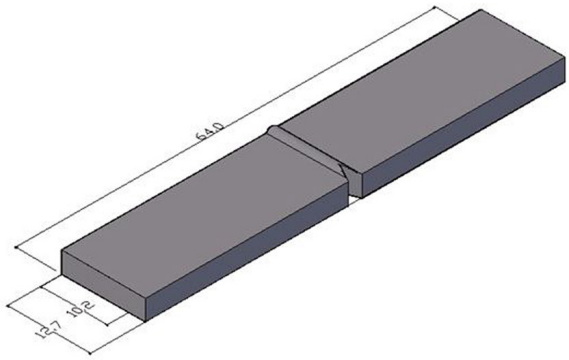

Fig. 2. Schematic of sample used for impact test.

3.6 Developing the design matrix and evaluation of the statistical model

The experiments were designed based on a four-factor three-level box-behnken design with 3 replication. The design expert software version 7 was used to develop the design matrix. To avoid any systematic error, experiments were randomly carried out as shown in Table 3. RSM is utilized to analyze the response and fit the best model on the response. The sequential F-test, lack of fit test and other adequacy measures were performed to evaluate and select the best fit.

3.7 Characterization and testing

Izod impact test was performed with notched specimens (Fig. 2) according to standard D256 [19]; using a Zwick 4100 machine with energy of 1J. The reported measured values are average of at least three measurements.

The morphology of impact fracture surfaces of the TPO nanocomposites was observed by scanning electron microscopy (SEM) at room temperature. A Philips XL30 SEM was used to collect SEM images for the nanocomposites specimens. The samples were etched by n-heptane and coated with a conductive gold thin layer.

X-ray diffraction (XRD) equipment was employed to evaluate the dispersion of nanoclay in the PP/EPDM matrix.

Analysis by XRD was performed at room temperature on a Philips model X'Pert diffractometer using radiation (wavelength) generated at 50 kV and 40 mA. The scanning rate was in wide angle mode for the range from 0 to 10.

Table 3. Design matrix and the measured response.

Run order	Input parameter level				Measured output
	C (wt%)	P (watt)	V (mm.min^{-1})	S (mm)	Impact strength (J/m)
1	3.00	100.00	1100.00	5.00	21.3 ± 0.5
2	0.00	120.00	750.00	6.50	40 ± 0.9
3	3.00	100.00	750.00	6.50	42.2 ± 07
4	3.00	80.00	750.00	5.00	29.7 ± 1
5	6.00	80.00	750.00	6.50	9.4 ± 0.6
6	6.00	100.00	750.00	8.00	30.6 ± 0.3
7	3.00	100.00	1100.00	8.00	25.6 ± 0.5
8	6.00	100.00	1100.00	6.50	3.4 ± 0.8
9	3.00	120.00	400.00	6.50	30 ± 1.1
10	3.00	100.00	400.00	5.00	31.3 ± 0.4
11	0.00	80.00	750.00	6.50	31.2 ± 0.7
12	0.00	100.00	750.00	8.00	56.3 ± 0.5
13	6.00	100.00	750.00	5.00	9.7 ± 0.3
14	0.00	100.00	1100.00	6.50	26.6 ± 0.2
15	3.00	80.00	1100.00	6.50	7.8 ± 0.9
16	3.00	100.00	750.00	6.50	44.7 ± 0.5
17	3.00	100.00	400.00	8.00	67.2 ± 0.4
18	0.00	100.00	400.00	6.50	49.1 ± 0.6
19	6.00	100.00	400.00	6.50	28.4 ± 0.8
20	3.00	120.00	750.00	8.00	57.1 ± 1.2
21	3.00	80.00	750.00	8.00	38.4 ± 3.2
22	6.00	120.00	750.00	6.50	8.1 ± 0.9
23	3.00	120.00	1100.00	6.50	23.4 ± 0.2
24	3.00	100.00	750.00	6.50	46.6 ± 0.4
25	3.00	100.00	750.00	6.50	47.5 ± 0.5
26	0.00	100.00	750.00	5.00	36.9 ± 0.5
27	3.00	100.00	750.00	6.50	44.1 ± 0.4
28	3.00	80.00	400.00	6.50	39.4 ± 0.6
29	3.00	120.00	750.00	5.00	20.3 ± 0.3

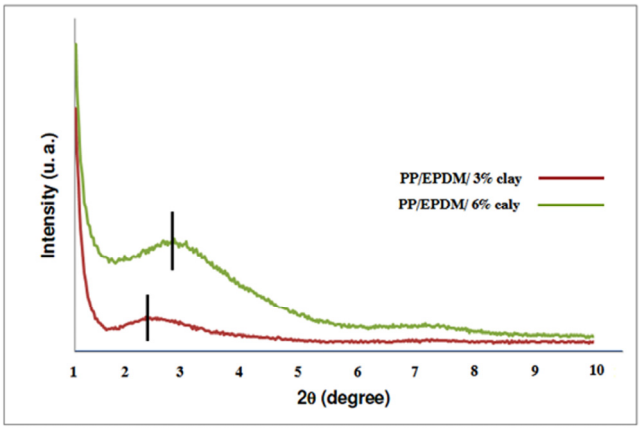

Fig. 3. XRD patterns of TPO nanocomposites in different loading of nanoclay.

4 Results and discussion

4.1 XRD analysis

The results of X-ray diffraction, a nano composite with cloisite 15A is shown in Figure 3. The neat nanoclay exhibits an intensive peak at $2\theta = 2.9°$.

4.2 Development of statistical model

The fit summary tab (Tabs. 4–6) in the design expert software suggests the highest order polynomial where the additional terms are significant and the model is not aliased. The sequential F-test for significance of both the regression model and the individual model terms along with the lack of fit test were carried out using the same software. Also, the model summary statistics recommended that the model with maximized R-squared and predicted R-squared is suitable. So, according to the information presented in Tables 4–6, a quadratic model can be used for prediction of impact strength and further analysis. The adequacy of the developed model was tested using the analysis of variance (ANOVA) technique and the results of second order response surface model fitting in the form of ANOVA are given in Table 7. The determination coefficient (R^2) indicates the goodness of fit for the model. The value of the R^2 indicates that only less than %2 of the total variations are not explained by the model. The value of adjusted determination coefficient (adjusted $R^2 = 0.9782$) is also high, which indicates a high significance of the model. Predicted R^2 is also in a good agreement with the adjusted R^2. Adequate precision compares the range of predicted values at the design points to the average prediction error. At the same time a relatively lower value of the coefficient of variation

Table 4. Sequential model sum of squares for selecting the highest order polynomial for impact strength model.

Source	Sum of Squares	*df*	Mean Square	*F* Value	*p*-value Prob > *F*	
Mean vs Total	30878.75	1	30878.75			
Linear vs Mean	4825.55	4	1206.39	12.23	<0.0001	
2FI vs Linear	630.92	6	105.15	1.09	0.4053	
Quadratic vs 2FI	1644.98	4	411.24	62.92	>0.0001	Suggested
Cubic vs Quadratic	44.19	8	5.52	0.70	0.6878	Aliased
Residual	47.32	6	7.89			
Total	38071.69	29	1312.82			

Table 5. Lack of Fit Tests for selecting the model with insignificant lack-of-fit.

Source	Sum of Squares	*df*	Mean Square	*F* Value	*p*-value Prob > *F*	
Linear	2349.85	20	117.49	26.78	0.0029	
2FI	1718.93	14	122.78	27.99	0.0027	
Quadratic	73.95	10	7.40	1.69	0.3244	Suggested
Cubic	29.77	2	14.88	3.39	0.1375	Aliased
Pure Error	17.55	4	4.39			

Table 6. Model Summary Statistics for focus on the model maxmizing adjusted R-squared and the predicted.

Source	Std. Dev.	R-Squared	Adjusted R-Squared	Predicted R-Squared	PRESS	
Linear	9.93	0.6709	0.6160	0.5382	3321.70	
2FI	9.82	0.7586	0.6245	0.4438	4000.68	
Quadratic	2.56	0.9873	0.9746	0.9370	453.39	Suggested
Cubic	2.81	0.9934	0.9693	0.4003	4313.94	Aliased

Table 7. ANOVA analysis for the weld impact model.

Source	Sum of Squares	*df*	Mean Square	*F* Value	*p*-value Prob > *F*	
Model	7097.76	11	645.25	115.24	<0.0001	significant
C	1887.52	1	1887.52	337.12	<0.0001	
P	44.08	1	44.08	7.87	0.0122	
V	1570.94	1	1570.94	280.58	<0.0001	
S	1323.00	1	1323.00	236.29	<0.0001	
CP	25.50	1	25.50	4.55	0.0477	
PV	156.25	1	156.25	27.91	<0.0001	
PS	197.40	1	197.40	35.26	<0.0001	
VS	249.64	1	249.64	44.59	<0.0001	
C^2	880.45	1	880.45	157.25	<0.0001	
P^2	785.06	1	785.06	140.21	<0.0001	
V^2	482.07	1	482.07	86.10	<0.0001	
Residual	95.18	17	5.60			
Lack of Fit	77.63	13	5.97	1.36	0.4154	not significant
Pure Error	17.55	4	4.39			
Cor Total	7192.94	28				
Std. Dev.	2.37		R-Squared		0.9868	
Mean	32.63		Adj R-Squared	0.9782		
C.V. %	7.25		Pred R-Squared	0.9525		
PRESS	342.02		Adeq Precision	42.878		

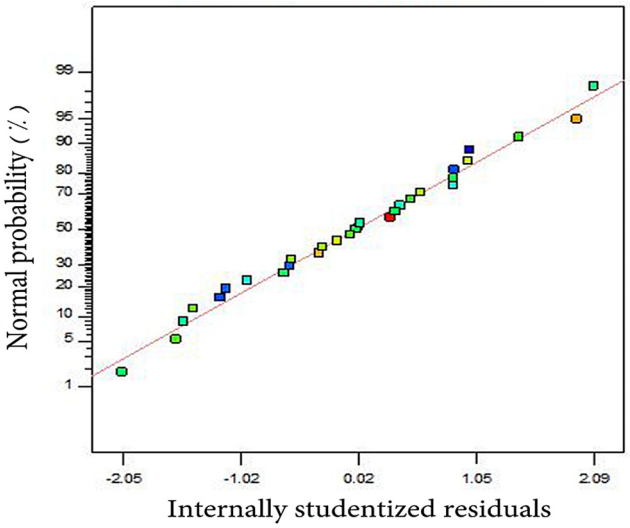

Fig. 4. Normal probability plot of residuals.

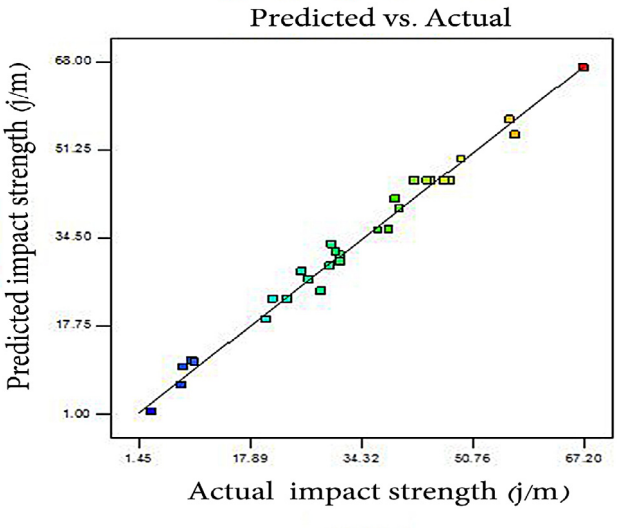

Fig. 5. plot of actual versus predicted responses.

(CV = 7.25) indicates improved precision and reliability of the conducted experiments.

The value of probability $> F$ in Table 6 for the model is less than 0.05 which indicates that the model is significant. In the same way, power (P), scan velocity (V), stand-off-distance (S), clay content (C), interaction effects of power with scan velocity (P × V), power with stand-off-distance (P × S), scan velocity with stand-off-distance (V × S) and second order terms of laser power (P^2), scan velocity (V^2) and clay content (C^2) have significant effect. Lack of fit is non significant as it is desired.

The final model to estimate impact strength of weld joint within determined design space in the coded and actual forms are represented in Equations (3), (4) respectively:

(a) in terms of coded factors:

$$\begin{aligned}\text{impact strength (J/m)} &= 45.34 - 12.54\text{C} + 1.92\text{P} \\ &- 11.44\text{V} + 10.50\text{S} - 2.52\text{C} \times \text{P} + 6.25\text{P} \times \text{V} + 7.03\text{P} \times \text{S} \\ &- 7.90\text{V} \times \text{S} - 11.44 \times \text{C}^2 - 10.80 \times \text{P}^2 - 8.47 \times \text{V}^2 \end{aligned} \quad (3)$$

(b) in terms of actual factors:

$$\begin{aligned}\text{impact strength (J/m)} &= -159.87409 + 7.65458\text{C} \\ &+ 3.43171\text{P} + 0.079489\text{V} - 5.13095\text{S} - 0.042083\text{C} \times \text{P} \\ &+ 8.92857 \times 10^{-4} \times \text{P} \times \text{V} + 0.23417\text{P} \times \text{S} - 0.015048\text{V} \times \text{S} \\ &- 1.27113 \times \text{C}^2 - 0.027007 \times \text{P}^2 - 6.91037 \times 10^{-5} \times \text{V}^2 \end{aligned} \quad (4)$$

The normal probability plot of the residuals for impact strength shown in Figure 4 reveals that the residuals are scattered around the straight line, which means the errors have been distributed normally. All the above considerations indicate adequacy of the regression model validation of the developed model.

To validate the developed model, three confirmation experiments under new conditions other than those used in the design matrix were carried out within the investigated range. For the actual response, the average of three measured results was calculated and the predicted value was calculated by substituting these conditions into the developed model. Table 8 summarizes the new experimental conditions, the average of actual experimental values, the predicted values and the percentage of error. Small percentage of error demonstrates that the estimated values are in good agreement with experimental values and the developed model can predict nearly accurate results.

Each expressed actual value in design matrix is compared with the predicted value calculated from the model in Figure 5. This figure is another reason for adequacy of the developed model because the data points are close to the 45° line.

Figure 6 is a perturbation plot which illustrates and also compares the effect of all the factors on the impact strength at the center point in the design space. It is clear from Figure 6 that all the four factors have a significant effect on the response. From this figure, it can be noticed that the impact strength decreases as the scan velocity increases. This is because increased velocity leads to low absorption of laser energy by the workpiece, causing smaller weld pool size. The smaller weld pool reduces the weld strength. In the case of laser power, the result indicates that maximum impact strength is obtained when laser power is at its center value. This behavior could be due to the fact that using high laser power increases power density, so larger weld pool size is obtained as a result of the heat input to the weld zone which increases the weld toughness. However; at very high laser power, the material may burn and partially decompose (Fig. 7) which reduces weld toughness. It can also be seen from the figure that as stand-off-distance increases, the impact strength also increases. The defocused beam or wider laser beam spreads over a wider area of the base material

Table 8. Validation test results.

Exp. No.	C (wt%)	P (watt)	V (mm/min)	S (mm)		Impact strength (J/m)
1	0	100	400	8	Actual	64.9
					Predicted	67.8
					Error %	–4.46
2	0	80	750	8	Actual	36.1
					Predicted	34.7
					Error %	+3.87
3	3	100	750	8	Actual	54.8
					Predicted	55.8
					Error %	–1.82

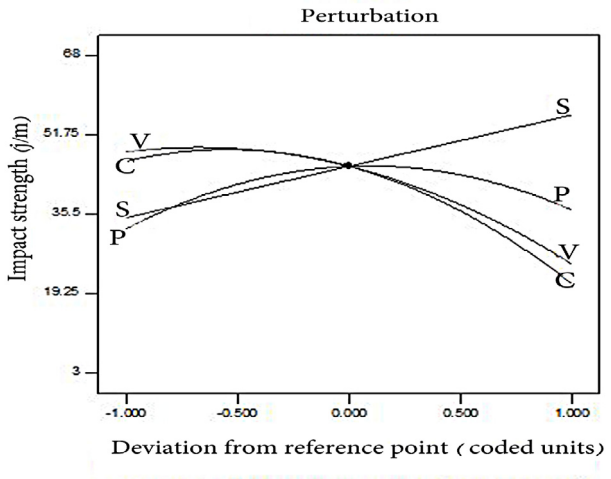

Fig. 6. Perturbation plot showing the effect of all factors on the impact strength.

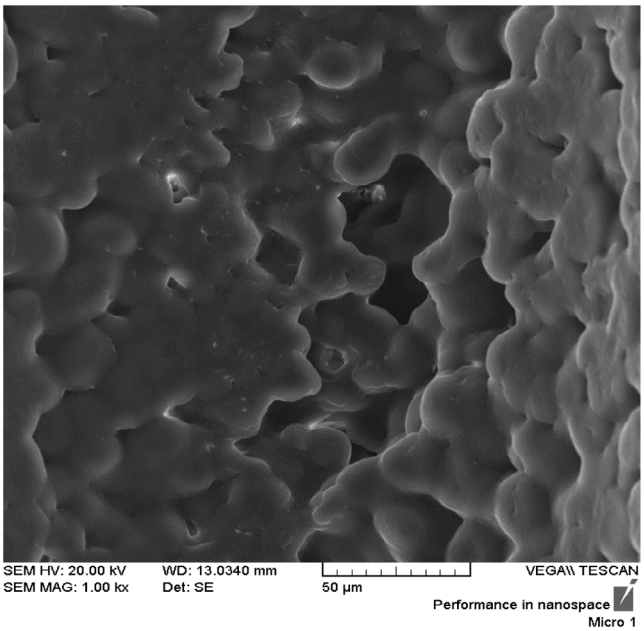

Fig. 7. Weld appearance due to overheating and decomposition.

which results to an increased weld-seam width and decrease of penetration depth. Weld penetration determines the stress-carrying capacity of a weld joint. Therefore decreased penetration leads to lower strength of the weld joint.

In Figure 6, increase of clay content on PP/EPDM matrix has a negative effect on impact strength of welds. The reason for this behavior can be attributed to agglomeration of clay particles in PP/EPDM matrix (the system) in high loading of nanoclay. Generally, mechanical properties of nanocomposites are related to dispersion condition of fillers, especially nanoclay particles [1–3,8,20]. Clay particles make stress concentration on matrix around nanoclay. So, these particles introduce small crack in matrix when specimen is under impact loading [3, 4, 21]. On the other hand, as loading of clay nanoparticles increases, the reinforcement effect of nanoclay increases which causes an enhancement in brittleness of the matrix [1–3,8]. It should be mentioned that a significant reduction in impact strength of TPO6 occurred in comparison to TPO3, which can be attributed to the more agglomeration of nanoparticles and inadequate dispersion of nanoparticles in matrix with 6%wt nanoclay. High level of impact strength in PP/EPDM matrix may be attributed to proportion of rubber droplet size in PP/elastomer blend [3,8]. When adding nanoclay, the size of EPDM droplets decreases due to increase of melt viscosity and the effect of clay particles in preventing coalescence of EPDM particles during processing [2,8]. High decrease of elastomer phase results in drop of impact strength of welds. This reduction will be extensive at higher loading of clay particles.

Figure 8 shows the interaction effect of P and V on weld impact strength. It is evident that, approximately at all levels of power, impact strength decreases as the scan velocity increases. This is due to the decrease in line energy. Line energy is the ratio of laser power to welding speed, defined as laser input energy per unit length [22]. Decreasing line energy at high speed and low power is more significant, therefore drop of impact strength is more extensive. So, using high speed with low laser power is not recommended. The results show at higher laser power, increase of speed has slight effect on impact strength, because high power overcomes the decreasing value of line energy as a result of high speed. The high line energy due to power of 120 W causes partial decomposition of material which leads to decrease of impact strength of welds.

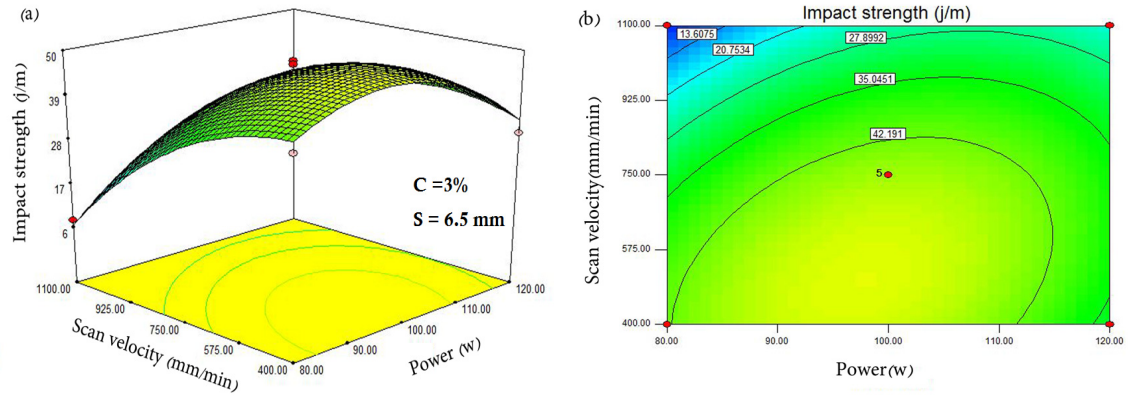

Fig. 8. Interaction effect of laser power and scan velocity on impact strength of weld when other parameters are fixed at center values. (a) The response surface and (b) the contour plot.

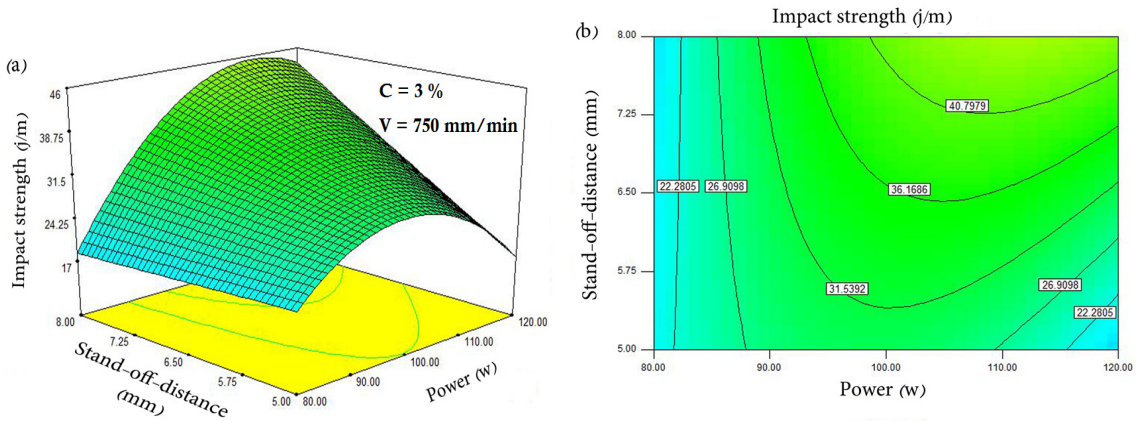

Fig. 9. Interaction effect of laser power and stand-off-distance on impact strength of weld when other parameters are fixed at center values. (a) The response surface and (b) the contour plot.

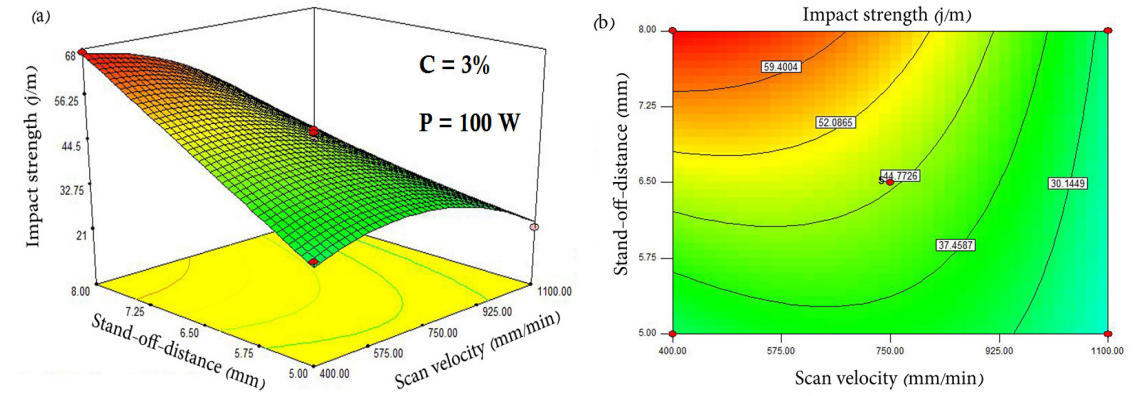

Fig. 10. IInteraction effect of scan velocity and stand-off-distance on impact strength of weld when other parameters are fixed at center values. (a) The response surface and (b) the contour plot.

Based on the above discussion, optimal impact strength of welds would be obtained when power of 100 W and scan velocity of 400 mm.min^{-1} are used.

Interaction effect of P and S is shown in Figure 9. This figure demonstrates improvement in impact strength with increasing both P and S. As explained previously, high ratio of depth of penetration to width in weld causes stress concentration on weld-seam [23, 24] and this phenomena decreases impact strength. Therefore with increasing stand-off-distance or spot size of laser beam, width of weld seam increases, resulting in a low ratio of depth to weld width which leads to low stress concentration on weld seam. On the other hand, decrease of power density as a result of increase of stand-off-distance can be addressed when selecting higher level of power to achieve adequate penetration. Using stand-off-distance of 5 mm at all levels of laser power decreases impact strength because although full penetration occurs, but the ratio of depth to width isn't appropriate.

Figure 10 shows the interaction effect of the V and S on the impact strength of welds. It is clear that lower speed and higher stand-off-distance result in a greater impact strength of welds. As mentioned earlier, increasing the stand-off-distance at lower speed improves the ratio of depth to width and decreases stress concentration on weld-seam leading to better impact strength. Although at higher speed of 850 mm.min^{-1}, the effect of stand-off-distance on impact strength would be slight. As the results indicate, very high speed and very low stand-off-distance are not recommended.

5 Conclusions

1. Laser butt welding of PP/EPDM/Nanoclay can be done successfully with proper selection of input variables. A quadratic model established by the RSM can predict weld impact strength satisfactorily.
2. The clay content has a greater influence on impact strength, followed by velocity, stand-off-distance and laser power.
3. With increasing clay content to PP/EPDM matrix from 0 to 6% wt, impact strength of welds decreased.
4. The impact strength increases as the laser power increases from 80 W to100 W and then decreases as the power starts to increase above 100 W.
5. Increase in velocity from 400 mm.min^{-1} to 1100 mm.min^{-1} decreased the impact strength from 48.31j to 25.43 j.
6. Increase in stand-off-distance from 5 to 8 mm increased the impact strength from 34.81 j to 55.67j.
7. According to the developed model, the highest predicted impact strength of 70 J/m is achieved at laser power of about 103W, velocity of 400 mm.min^{-1}, stand-off-distance 8mm and clay content of about 1.3% wt.

References

[1] K. Sridevi, S. Soundararajan, K. Palanivelu, J. Polym. Mater. 28 (2011) 171–185
[2] H.-S. Lee, P.D. Fasulo, W.R. Rodgers, D.R. Paul, Polymer 46 (2005) 11673–11689
[3] I. Hejazi, J. Seyfi, G. Mir Mohamad Sadeghi, S.M. Davachi, Mater. Design 32 (2010) 649–655
[4] J.K. Mishra, K.J. Hwang, C.S. Ha, Polymer 46 (2005) 1995–2002
[5] D.R. Paul, L.M. Robeson, Polymer 49 (2008) 3187–3204
[6] G. Naderi, P.G. Lafleur, C. Dubois, Polym. Compos. 29 (2008) 1301-1309
[7] R. Khosrokhavar, G. Naderi, G. Bakhshandeh, M.H.R. Ghoreishy, Iranian Polym. J. 20 (2010) 41–53
[8] I. Hejazi, F. Sharif, H. Garmabi, Mater. Design 32 (2011) 3803–3809
[9] N. Amanat, N.L. James, D.R. McKenzie, Medical Eng. Phys. 32 (2010) 690–699
[10] P.J. Bates, C. Braybrook, T. Kisway, B. Tucker, T.G. Gopakumar, D.J.Y.S. Pagé, C.Y. Wu, ANTEC 1 (2004) 1128–1131
[11] A. Mokhtarzadeh, A. Benatar, C.Y. Wu, ANTEC 1 (2004) 1168–1172
[12] L. Dosser, K. Hix, K. Hartke, R. Vaia, M. Li, Proceed. SPIE 5339 (2004) 465–474
[13] M.R. Nakhaei, N.B. Mostafa Arab, G. Naderi, M. Hoseinpour Gollo, J. Mech. Sci. Technol. 27 (2013) 843–848
[14] M.R. Nakhaei, N.B. Mostafa Arab, G. Naderi, Iran Polym. J. 22 (2013) 351–360
[15] B. Acherjee, A.S. Kuar, S. Mitra, D. Misra, S. Acharyya, Optics Laser Technol. 44 (2012) 1372–1383
[16] X. Wang, C. Zhang, K. Wang, P. Li, Y. Hu, K. Wang, H. Liu, Optics Laser Technol. 44 (2012) 2393–2402
[17] H.A. Eltawahni, A.G. Olabi, K.Y. Benyounis, Mater. Design 31 (2010) 4029–4038
[18] H. Liu, K. Wang, P. Li, C. Zhang, D. Du, Y. Hu, X. Wang, Optics Lasers Eng. 50 (2012) 440–448
[19] Standard test methods for determining the izod pendulum impact resistance of plastics (ASTM), D256, 2004
[20] R.R. Tiwari, D.R. Paul, Polymer 52 (2011) 5595–5605
[21] J.Z. Liang, Polym. Bull. 6 (2010) 815–824
[22] G. Zak, L. Mayboudi, M. Chen, P.J. Bates, M. Birk, J. Mater. Process. Technol. 21 (2010) 24–31
[23] welding handbook eighth edition, volume 2, welding processes, pp. 726–727
[24] welding metallurgy second edition, sindo kou, pp. 294–295